Theoretical Chemistry Accounts (2021) 140:119
https://doi.org/10.1007/s00214-021-02823-z

REGULAR ARTICLE

Improvement of floxuridine anti-cancer adsorption on boron carbonitride nanotubes with iron doping: a theoretical study

Fazlolah Eshghi[1] · Zainal Ghahramani[2] · Reza Ghoreishi[3] · Sahar Ghahremani[4]

Received: 4 April 2021 / Accepted: 31 July 2021 / Published online: 7 August 2021

Abstract

Nowadays, nanotubes are regarded as one of the most important carriers to transfer drug into target cell without side effects. In this study, low-lying structures of single-wall boron carbonitride nanotube (SWBCNNT) as a novel class of carriers have been investigated using M06-2X/6-31 + g(d) method after DFT calibration. With regard to mixing patterns for SWBCNNT formation, **L(BN) R(C)3** nanotube has selected as candidate structure due to more negative value of mixing energy. So, Fe-doping in this nanotube is carried out to have strong floxuridine (FUDR) anti-cancer adsorption and better drug delivery. Global chemical reactivity indices can help to select suitable doping position; these indices show that doping instead carbon (**Fe–C{L(BN) R(C)3}** nanotube) causes the most tendency for interaction with the FUDR anticancer. Besides, local reactivity descriptors show that favorable active sites of anticancer for nucleophilic attacks are oxygen (O5 and O6) and nitrogen (N7) atoms. Furthermore, comparing of adsorption energies shows that selected doped nanotube has strong interaction with mentioned active sites of FUDR anticancer in perpendicular orientation. This issue is confirmed by their adsorption energies values and significant donor–acceptor charge transfers. Therefore, **Fe–C{L(BN) R(C)3}** nanotube is proposed as favorable carrier to FUDR anticancer transfer into target cells.

Keywords Mixing energy · Floxuridine anticancer · Boron carbonitride nanotube · Binding energy · Drug delivery

1 Introduction

Floxuridine (FUDR) with pyrimidine structure has attracted much attention due to its great applications such as inhibitory, antimetabolites, advanced colon, kidney, hepatic arterial infusion, and stomach cancer treatment [1]. How to transfer FUDR drug into target cells is an important point due to its side effects such as decreasing white and red blood cells and levels of platelets [2]. Some research groups were proposed endogenous serum albumin to transfer and delivery of FUDR drug [2, 3]. In another study, the self-assemblies of the FUDR-containing DNA and RNA nano-gels were introduced as drug delivery systems [4]. Therefore, selection of favorable carrier is an important challenge in cancer therapy due to decrease in side effects [5, 6].

In recent years, nano-materials were introduced as reliable carriers to transfer drug molecules into target cells such as boron nitride (BN) and carbon (C) nanotubes. Combining both types of nanotubes results in producing a novel nanotube with more and better applications. Many research groups experimentally have been synthesized this novel nanotube as ternary B–C–N nanotube ($C_x(BN)_y$ or BC_2N or

✉ Fazlolah Eshghi
Feshghi1983@gmail.com

Zainal Ghahramani
eili627@yahoo.com

Reza Ghoreishi
rezaghoreishi2010@yahoo.com

Sahar Ghahremani
Fazlolah_1982@yahoo.ca

[1] Department of Chemistry, College of Science, Shiraz University, Eram Square, Eram Street, Shiraz 7146713565, Iran

[2] Department of Chemistry, Islamic Azad University, Firoozabad Branch, Firoozabad, Iran

[3] Department of Chemistry, Islamic Azad University, Rasht Branch, Rasht, Iran

[4] Department of Chemistry, Islamic Azad University, Central Tehran Branch, Tehran, Iran

BCNNT) [7–15]. In addition, there have been several theoretical studies on optical, electronic, and elastic properties of the BC_2N nanotubes [16–24]. For example, both zigzag and armchair nanotubes were studied in order to investigate energetics and electronic properties [25]. In another studies, adsorption of amino acids was investigated with the aim of biotechnological applications and nano-devices [26, 27]. In fact, the BC_2N nanotubes with high polarity and surface-to-volume ratio, magnetic behavior, and low-chemical potential are suggested for drug delivery applications [19, 28]. That's why, single-wall BC_2N nanotube (SWBCNNT) is considered as building block in current study.

Doping of metal in SWBCNNTs can change its behavior in interaction with other molecules due to change of electrostatic potentials in the inner/outer surface [28, 29]. For instance, Si-doping in SWBCNNTs leads to sensing of the presence H_2CO molecule due to increase in the electric conductivity of nanotube [30]. In another report, this doping decreases formation energy of SWBCNNTs in comparison with CNT and BNNTs [31]. In current study, we have doped the Fe-metal into the SWBCNNT structure because this metal maybe helps to solve the problem of anemia in cancer patients after drug delivery. However, serious side effect has not been reported for this doping on FUDR anticancer drug delivery. So, the aim of this study is to assess geometric and electronic candidate structures of Fe doped and un-doped SWBCNNTs. After this assay, influence of metal doping into FUDR adsorption will investigate by means of density functional theory (DFT).

2 Computational methods

Ground state structures have been investigated in the framework of density functional theory (DFT) implemented to Gaussian 09 program package [32]. M06-2X hybrid functional with all electron basis sets, 6–31 + G (d), is used in the optimization process after DFT calibration method [33–35]. In this method, selected exchange–correlation (*xc*) functional and basis set in comparison with the other xc functional (Table S1) calculates more exact bond length and frequency for studied molecules, more negative energy of ground state, and low spin contamination. Geometry optimization of structures is carried out without any symmetry constrains (C1 symmetry). With vibrational frequency test, it can be found that the optimized geometries stand in the local minima.

The propensity of boron, carbon, and nitrogen atoms to segregate and the formation of SWBCNNTs are calculated by mixing energy [36]. The more negative (less positive) values of the mixing energy indicate favorable mixing among the compositions and thus more stable nanotube [36]. Mixing (excess) energy, E_{mix} [36], is used in order to assess stability of SWBCNNTs with respect to their composition:

$$E_{\text{mix}} = E_{B_mC_nN_O} - \frac{m+O}{N}E_{B_mN_OC_0} - \frac{n}{N}E_{B_0N_0C_n} \quad (1)$$

where E_{mix} is mixing energy, and $E_{B_mC_nN_O}$, $E_{B_mN_OC_0}$, and $E_{B_0N_0C_n}$ are total energy of SWBCNNTs, pure SWBNNTs and SWCNTs. The N, *n*, *m, O* are number of total atoms in SWBCNNTs, number of carbon, boron, and nitrogen atoms, respectively.

Chemical reactivity of un-doped and doped SWBCNNTs with FUDR was calculated based on global and local reactivity descriptors. Global reactivity descriptors are electronic chemical potential ($\mu = -(IP + EA)/2$), chemical hardness ($\eta = (IP - EA)/2$), softness ($S = 1/\eta$), and electrophilicity ($\omega = \mu 2/2\eta$), respectively [37]. The μ is the escaping tendency of electrons; the η is a resistance to charge transfer; and the ω is floating of electron between nucleophile and electrophile. Local reactivity descriptors were only calculated to the most active site in favorable Fe-doped SWBCNNT and FUDR anticancer. Local Fukui function (f^+), local softness (s^+), and local philicity (ω^-) are clear-cut examples. The f^+, s^+, and the ω^- show active center to nucleophilic attacks.

Using three approach point methods, adiabatic ionization potential (IP) and electron affinity (EA) in above equations were calculated [38]:

$$IP_{\text{ad}} = E_{\text{total}}\left(\text{compound}^+\right) - E_{\text{total}}(\text{compound}) \quad (2)$$

$$EA = E_{\text{total}}(\text{compound}^-) - E_{\text{total}}(\text{compound}) \quad (3)$$

where $E_{\text{total}}(\text{compound})$, $E_{\text{total}}\left(\text{compound}^+\right)$, and $E_{\text{total}}(\text{compound}^-)$ are total energy of natural, cationic, and anionic compound (SWBCNNT or FUDR), respectively.

Stability of the complexes is evaluated by binding energy factor in the following form:

$$E_{\text{bind}} = E_{\text{complex}} - \left(E_{\text{Fe - C\{SWBCNNT\}}} + E_{\text{FUDR}}\right) \quad (4)$$

In this equation, E_{complex}, $E_{Fe-C\{\text{SWBCNNT}\}}$, and E_{FUDR} are the total energy of complex, the Fe–C{SWBCNNT}, and floxuridine.

Depletion of occupancies, percent of Lewis and non-Lewis and stabilization energies (E^2_{ij}) [39, 40] as complementation of geometric information are obtained by natural bond orbital (NBO) analysis:

$$E_{ij}^2 = \frac{\left|i\left|\hat{H}\right|j\right|^2}{E_j - E_i} \quad (5)$$

where $\hat{H}$ is interaction Hamiltonian, E_j and E_i are orbital energies, and $\langle\left|\hat{H}\right|\rangle$ is the matrix element.

3 Results and discussion

3.1 Geometric and electronic analysis

Low-lying structures of FUDR and possible SWBCNNTs geometries were investigated using M06-2X/6–31G* level of theory, as shown in Fig. 1. Geometry optimization shows that the B–N, B–C, C–C, and C–N bond lengths in open end SWBNNTs are 1.438, 1.498, 1.400, and 1.409 Å, respectively; this result is in good agreement with other reports [41–45]. Performance and reactivity of SWBCNNTs can be tuned by controlling their structures, composition, and size. For instance, **L(BN) R(C)3** geometry has less positive value of mixing energy in comparative to two structure of nanotubes, see Table 1. In addition, the least relative energy is belonging to this nanotube. Therefore, this nanotube has more stability than two BC_2N nanotubes. So, we consider this geometry as favorable candidate structure in order to doping of Fe-metal and interaction with FUDR anticancer in current study.

For improvement of FUDR anticancer adsorption and better drug delivery, one Fe-metal was doped on **L(BN) R(C)3** nanotube. There are three possible centers for Fe-metal doping in this nanotube, see Fig. 1. Fe-doping instead carbon (Fe–C) and boron or nitrogen atoms (Fe–B and Fe–N) causes high and low localization of electrons in closed- and open-shell systems. In fact, metal doping results in changing in energetic, geometric, and electronic parameters in SWBCNNTs. For example, negative relative energy of the Fe–N- and Fe–B-doped nanotubes than Fe–C structure indicates more stability of them, see Table 2. Besides, changing in the X–Fe (X = B, C, and N) bond lengths leads to changing of dipole moments and creation conditions for effective interaction with anticancer molecule. The least changing of dipole moments was seen in the Fe–N- and Fe-B-doped nanotubes in comparative to selected un-doped nanotube, see Table 2. So, these structures are probably high stability than Fe–C-doped nanotube and low tendency for interaction with FUDR anticancer. Furthermore, global and local reactivity descriptors were calculated to confirm above results.

Reactivity descriptors investigate role of molecules and active sites in their reaction; these indices were calculated for un-doped, doped SWBCNNTs, and FUDR molecules, see Table 3. With regard to this table, both **L(BN) R(C)3** and **Fe–C{L(BN) R(C)3}** structures have more negative chemical potential than others; so, they rarely loss electron

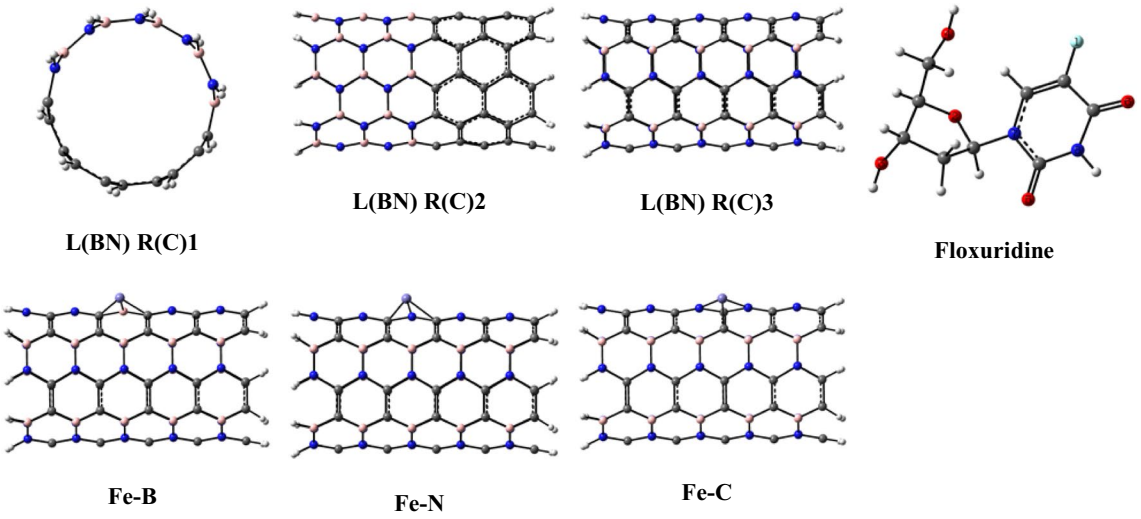

Fig. 1 Optimized geometry structures of un-doped and doped SWBCNNTs and floxuridine anticancer in M06-2X/6–31G* level of theory

Table 1 Calculated stability of local minimum (**ΔE**) and mixing energy ($\mathbf{E}_{mixing}$) in kcal mol^{-1}, dipole moment (Debye), and bond length (Å) of possible structures of un-doped SWBCNNTs

Compounds	Δ*Em*	E_{mixing}	Dipole	r_{B-N}	r_{B-C}	r_{C-C}	r_{C-N}
L(BN) R(C)1	+23.4	164.2	45.029	1.427	1.474	1.388	1.417
L(BN) R(C)2	+148.6	289.4	0.749	1.419	1.436	1.409	1.381
L(BN) R(C)3	0.0	140.8	1.042	1.438	1.498	1.400	1.409

Δ*Em* is relative mixing energy

and play the electrophile role in the reaction. Among doped and un-doped nanotubes, the least chemical hardness (0.08 eV) and the most softness (12.50 eV) values belong to **Fe–C{L(BN) R(C)3}** structure; so, this doped nanotube has high tendency for interaction with nucleophile. On the other hand, FUDR as ligand with the most chemical hardness (3.94 eV) plays the nucleophile role in reaction with selected Fe-doled nanotube. Finally, the most (123.77 eV) and least (1.91 eV) values of electrophilicity belong to **Fe–C{L(BN) R(C)3}** (as electrophile) and ligand (as nucleophile); this issue confirms that the floating of electron is between these compounds.

Local reactivity descriptors of **Fe–C{L(BN) R(C)3}** and FUDR structures are used to find active sites and better understanding interaction, as given in Table 4. With regard to this table, the highest local Fukui function (f^+) and local philicity (ω^+) descriptors belong to the Fe center in **Fe–C{L(BN) R(C)3}** nanotube. So, this atom is active center in the nucleophilic attacks. On the other hand, more positive value of s^+ and Δs in metal center of **Fe–C{L(BN) R(C)3}** nanotube shows existence suitable condition for nucleophile attacks of FUDR. In fact, nucleophile attacks are mainly due to high local softness and dual softness in the oxygen (O5 and O6) and nitrogen (N7) centers in FUDR anticancer molecule. Herein, we have considered these atoms as nucleophile centers in interactions with **Fe–C{L(BN) R(C)3}** nanotube**.**

Molecular electrostatic potential (MEP) maps can help to confirm reactivity results and investigate interactions. Fe–X{SWBCNNTs, X = B, C, and N} and FUDR anticancer maps are plotted in Fig. 2. High and low electron densities are related to negative and positive regions, respectively.

Table 2 Hartree–Fock energy, relative local minimum energy, bond length (Å), dipole moment, and difference dipole moment with un-doped nanotube (Debye) of favorable Fe-doped SWBCNNTs (**Fe–X{L(BN) R(C)3}, *x* = B, C, and N**)

Compounds	EHF	Δ*Em*	$r_{\text{Fe-B}}$	$r_{\text{Fe-C}}$	$r_{\text{Fe-N}}$	Dipole	ΔDipole*
Fe–B	−5017.482953	−4.2	–	1.698 (1.426)	1.816	1.967	0.925
Fe–C	−5018.996366	0.0	1.733 (1.638)	1.695	–	10.265	9.223
Fe–N	−5030.510306	−17.3	1.566	1.749 (1.657)	–	1.513	0.471

Δ*Em* is relative local minimum energy

*Ground state dipole of **L(BN) R(C)3** is 1.042 Debye

Table 3 Global reactivity descriptors of un-doped and doped **L(BN) R(C)3** and floxuridine, HOMO–LUMO gaps in eV

Compounds	IP	EA	μ	$\lvert\eta\rvert$	S	ω	$\Delta H-L$	$\Delta H_{\text{L}}-L_{\text{NT}}$
L(BN) R(C)3	4.72	4.40	−4.56	0.16	6.25	64.98	9.11	12.22
Fe-B{L(BN) R(C)3}	3.37	3.18	−3.28	0.10	10.53	56.45	8.97	11.81
Fe–C{L(BN) R(C)3}	4.37	4.53	−4.45	0.08	12.50	123.77	8.90	11.35
Fe–N{L(BN) R(C)3}	4.02	3.49	−3.76	0.27	3.77	26.60	9.28	11.51
Floxuridine	7.82	−0.06	−3.88	3.94	0.25	1.91	7.86	–

Table 4 Local reactivity descriptors of un-doped and doped **Fe–C{L(BN) R(C)3}** and floxuridine for heteroatoms in eV

Compounds	Atoms	f+	F−	s+	s−	w+	w−	Δ*s*	Δ*ω*
Fe–C	Fe	0.2453	−0.7051	3.0665	−8.8141	30.3629	−87.2736	11.8806	117.6365
	B	0.0105	−0.0124	0.1312	−0.1555	1.2993	−1.5395	0.2867	2.8388
	C	0.0313	−0.0033	0.3915	−0.0412	3.8744	−0.4078	0.4327	4.2822
	N	−0.0086	0.0109	−0.1081	0.1360	−1.0704	1.3467	−0.2441	−2.4171
Floxuridine	F	0.0729	−0.0686	0.0182	−0.0171	0.1393	−0.1310	0.0354	0.2702
	O2	0.0162	0.0003	0.0041	0.0001	0.0310	0.0006	0.0040	0.0304
	O3	0.0097	−0.0069	0.0024	−0.0017	0.0186	−0.0133	0.0042	0.0318
	O4	−0.0029	0.0069	−0.0007	0.0017	−0.0055	0.0131	−0.0024	−0.0187
	O5	0.1953	−0.0868	0.0488	−0.0217	0.3729	−0.1658	0.0705	0.5387
	O6	0.1371	−0.1581	0.0343	−0.0395	0.2619	−0.3020	0.0738	0.5639
	N7	0.1891	−0.0192	0.0473	−0.0048	0.3612	−0.0367	0.0521	0.3979
	N8	0.0130	−0.0157	0.0032	−0.0039	0.0248	−0.0300	0.0072	0.0548

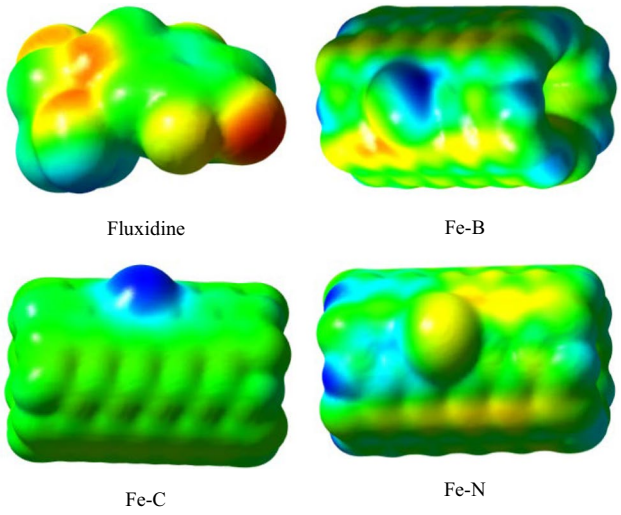

Fig. 2 Plotted molecular electrostatic potential (MEP) maps of floxuridine anticancer and Fe–X{SWBCNNTs, *X* = B, C, and N} in selected theoretical method

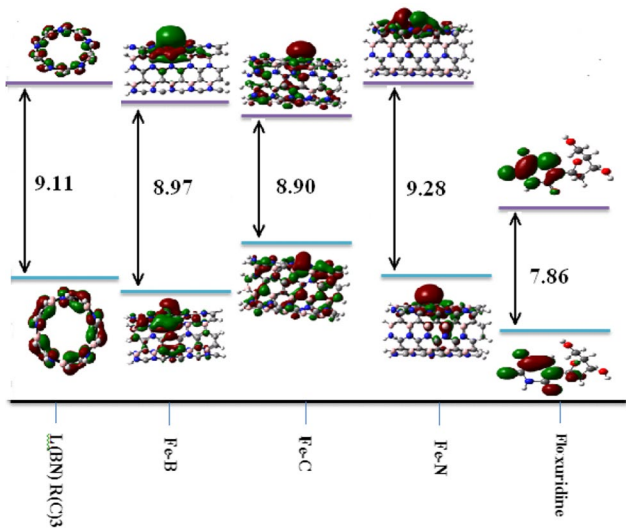

Fig. 3 Highest occupied molecular orbitals (HOMO) and lowest unoccupied molecular orbitals (LUMO) gap of un-doped and doped of **L(BN) R(C)3** and floxuridine anticancer. All presented energies are in eV

The yellow, blue, and green colors elucidate the most negative, positive, and zero electrostatic potential, respectively. According to Fig. 2, there are only two positive (blue color) and zero (green color) electrostatic potential regions in **Fe–C{SWBCNNT}** system. Positive point is belonging to Fe-metal site and shows electrophilic property of this atom; this issue confirms that Fe-doping instead carbon atom leads to increasing localization of electrons and electrophilic property in Fe center of **Fe–C{SWBCNNT}** system. So, adsorption and delivery of the FUDR anticancer by the **Fe–C{L(BN) R(C)3}** nanotube are probably carried out better than the Fe-B and Fe–N doped and un-doped nanotubes; this issue is due to being reliable of global reactivity descriptors and the MEP maps, see Table 3 and Fig. 2.

Highest occupied molecular orbitals (HOMO) and lowest unoccupied molecular orbitals (LUMO) gap is other reactivity parameter to show stability of nanotubes. Fe-doping partly results in decrease in the HOMO–LUMO gap in comparison with pure nanotube, especially **Fe–C{L(BN) R(C)3}**, see Table 3. According to this table and Fig. 3, decrease in $HOMO_{FUDR}$-$LUMO_{Fe\text{-}C\{L(BN)R(C)3\}}$ gap is mainly followed by better charge transfer between anticancer and nanotube. So, adsorption and delivery of FUDR anticancer are probably carried out better than other Fe-doped nanotubes, where this issue is in good agreement with previous results.

3.2 Adsorption of floxuridine anticancer on doped SWBCNNTs

Fe doped and un-doped BC_2N nanotubes were interacted with FUDR anticancer at parallel and perpendicular orientations in order to confirm previous results. Besides, introduced active sites in FUDR structure such as the O5 and O6 and N7 atoms are considered as the most possible interaction sites at perpendicular orientations, see Fig. 4 and Figure S1 (S means supplementary file). According to Table 5, the X–Fe (X = O, and N atoms of FUDR) distance at parallel orientations is longer than perpendicular orientations in FUDR-[Fe-SWBCNNTs] complexes. On the other words, long distance in parallel than perpendicular orientations is reflection of low adsorption energies. This issue is confirmed with more negative adsorption energy (E_{ads}) in perpendicular orientations, see Table 5. Furthermore, the most negative E_{ads} was shown in perpendicular orientations of FUDR-**Fe–C{L(BN) R(C)3}** complexes. So, according

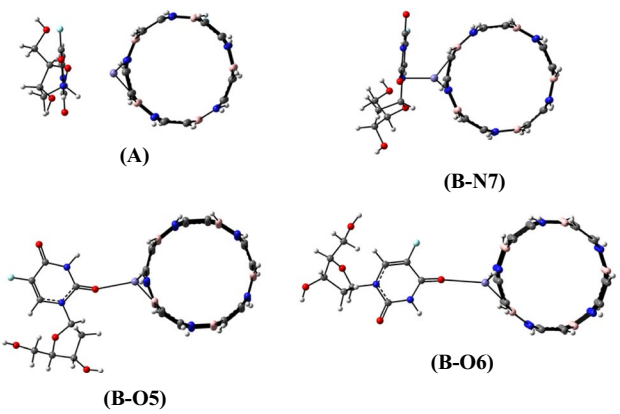

Fig. 4 Interactions of floxuridine and **Fe–C L(BN) R(C)3** in parallel (**A**) and perpendicular (**B**) orientations, respectively

Table 5 Adsorption (binding) energy in different methods (kcal mol^{-1}), distances (D, Å), and bond angles (degree, °) in parallel and perpendicular orientations (O and N sites)

Compounds	Orientation	E_{ads}(M06)	B3lyp	B97-d	D*	∠ Fe–X-Ph (X = O and N)**
Fe–B	Parallel	−9.8	−13.8	−12.5	2.749	85.4
	N7	−38.2	−32.7	−35.1	2.615	81.6
	O5	−14.0	−12.6	−10.0	2.561	161.2
	O6	−39.3	−38.9	−42.6	2.421	143.9
Fe–C	Parallel	−86.6	−81.4	−83.6	3.214	94.5
	N7	−92.5	−96.5	−87.8	2.531	88.3
	O5	−98.9	−102.6	−88.7	2.264	161.3
	O6	−91.7	−97.5	−98.8	2.788	163.0
Fe–N	Parallel	−47.8	−47.4	−58.6	3.263	94.7
	N7	−56.3	−53.7	−64.9	2.784	81.4
	O5	−62.8	−66.2	−68.7	2.218	150.1
	O6	−60.1	−59.9	−65.5	2.313	152.6
Un-doped	N7	−50.0	−54.6	−53.1	2.450	84.4
	O5	−51.0	−60.1	−59.3	2.262	160.1
	O6	−50.3	−57.8	−39.9	2.264	178.7

*D means interaction distance between FUDR and BCNNT

**∠ Shows angle

to this issue previous result can guess that the **Fe–C{L(BN) R(C)3}** nanotube will be probably favorable career for drug delivery.

On the other hand, repulsive interaction between anticancer and surface of nanotube in parallel orientation is greater than other. Therefore, binding of anticancer in the perpendicular orientations is stronger than other. The Fe–O–Ph bond angle is larger than Fe–N–Ph bond angle in perpendicular orientation of FUDR-BC_2N complexes; this issue can be reflecting of their stability and better drug delivery. More negative adsorption (binding) energies show the best orientation of their adsorptions, see Table 5. With regard to this table, less binding energy and more stability belongs to FUDR-**Fe–C{L(BN) R(C)3}** complex in perpendicular orientations (especially in O5 active site). This result is in good agreement with reactivity results.

Density of state (DOS) has been applied to analysis of the HOMO–LUMO gap of chemical structures for better understanding of FUDR anticancer adsorption on **Fe–C{L(BN) R(C)3}** nanotube. Total DOS of FUDR-**Fe–C{L(BN) R(C)3}** complex in perpendicular orientation is plotted in Fig. 5 and for other complexes is plotted in Figure S2. In fact, decrease in HOMO–LUMO gaps mainly results from low modification and reliable adsorption of drug molecule on BC_2N complexes. According to these figures, the most decreasing is belonging to FUDR-Fe–C{L(BN) R(C)3} complex. So, charge transfers between FUDR and **Fe–C{L(BN) R(C)3}** nanotube are conveniently carried out.

NBO-based calculation shows that there are significant charge transfers in perpendicular interaction; there is no any significant donor–acceptor interaction in parallel orientation. Total donor acceptors at the O5, O6, and N7 atoms of perpendicular orientations with delocalization energy based on second-order perturbation theory are 17.0, 19.8, and 21.1 kcal mol^{-1}. Total Lewis electron densities for the FUDR-**[Fe–C{L(BN) R(C)3}]** complexes are 97.22%, 97.12%, and 97.19%, of the idealized structure, respectively. Therefore, existence of significant charge transfers, low Lewis localization, and low occupancies confirms reliable interactions in perpendicular orientations.

4 Conclusion

In this study, after optimization processing of the un-doped BC_2N nanotubes, **L(BN) R(C)3** was selected as candidate structure for Fe-doping due to more negative mixing energy value. After Fe-doping instead carbon, nitrogen, and boron nanotube atoms, Fe–C{L(BN) R(C)3} was selected as candidate structure for interaction with drug molecule due to positive mixing energy (low stability) and high changing of dipole moment. In addition, global chemical reactivity indices imply that **Fe–C{L(BN) R(C)3}** structure has high tendency to interact with FUDR anticancer; this issue results from low chemical hardness, high chemical softness, and fast floating of electrons between these compounds. More importantly, high localization of electrons and low $HOMO_{FUDR}$-$LUMO_{Fe\text{-}C\{SWBCNNT\}}$ gap result in improvement in adsorption energies about 80% than un-doped nanotube. Besides, existence of several significant charge transfers with

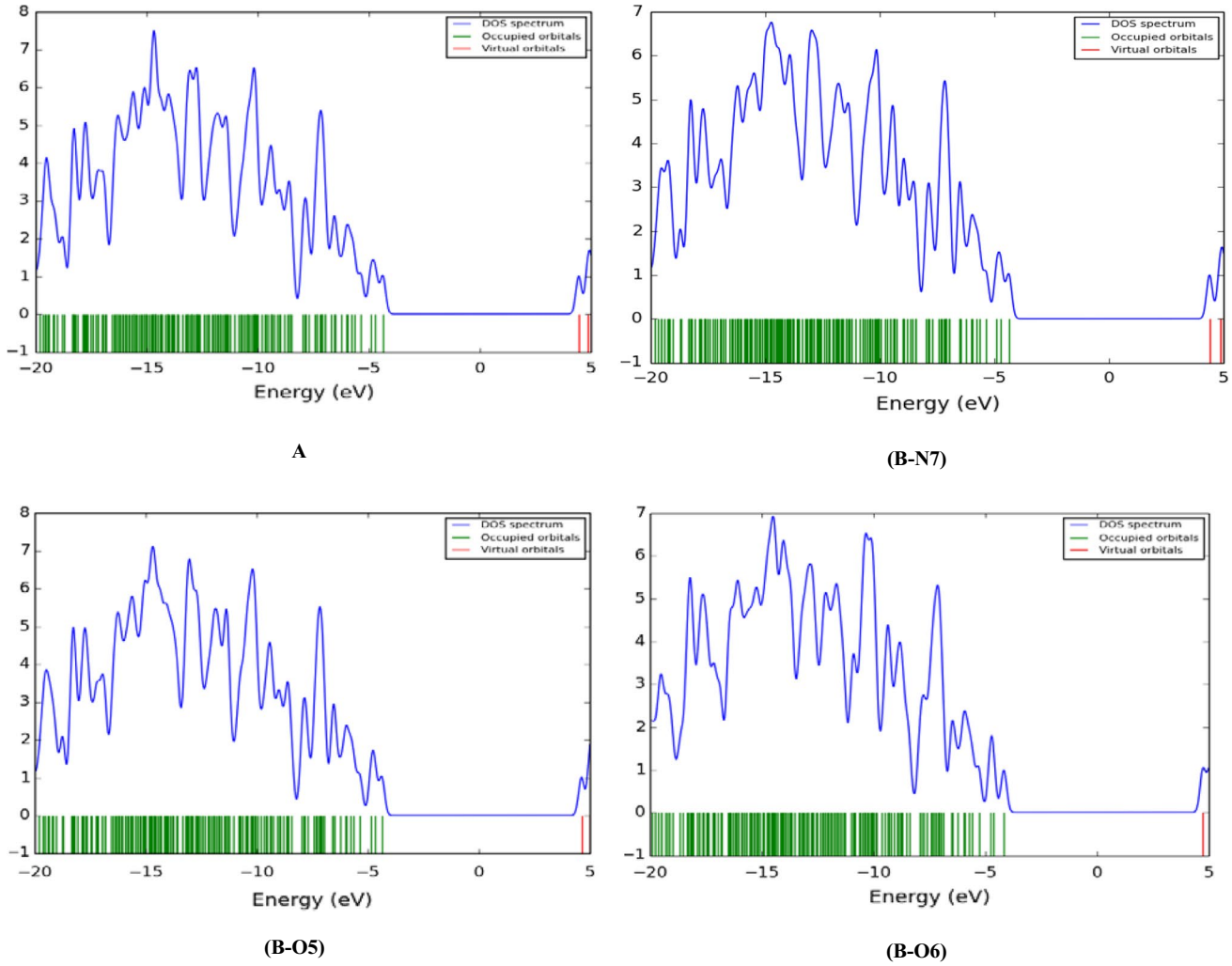

Fig. 5 Total density of state (DOS) of FUDR- **Fe–C L(BN) R(C)3** complexes in parallel (**A**) and perpendicular (**B**) orientations

high stabilization energy causes introducing of this nanotube as favorable carrier to transfer anticancer molecule.

Supplementary Information The online version contains supplementary material available at https://doi.org/10.1007/s00214-021-02823-z.

Data availability The data that support the findings of this study are available within supplementary material.

References

1. DG Power NE Kemeny 2009 The role of floxuridine in metastatic liver disease Mol Cancer Ther 8 1015 1025 https://doi.org/10.1158/1535-7163.MCT-08-0709
2. C Jin H Zhang J Zou 2018 Floxuridine homomeric oligonucleotides "hitchhike" with albumin in situ for cancer chemotherapy Angew Chem Int Ed 57 8994 8997 https://doi.org/10.1002/anie.201804156
3. W-S Yeo R Arya KK Kim 2018 The FDA-approved anti-cancer drugs, streptozotocin and floxuridine, reduce the virulence of Staphylococcus aureus Sci Rep 8 2521 https://doi.org/10.1038/s41598-018-20617-5
4. Y Ma H Liu Q Mou 2018 Floxuridine-containing nucleic acid nanogels for anticancer drug delivery Nanoscale 10 8367 8371 https://doi.org/10.1039/C8NR01226A
5. J You F-Q Hu Y-Z Du H Yuan 2008 Improved cytotoxicity of doxorubicin by enhancing its nuclear delivery mediated via nanosized micelles Nanotechnology 19 255103 https://doi.org/10.1088/0957-4484/19/25/255103
6. Y Luo MR Ziebell GD Prestwich 2000 A hyaluronic acid−taxol antitumor bioconjugate targeted to cancer cells Biomacromol 1 208 218 https://doi.org/10.1021/bm000283n
7. Y Miyamoto A Rubio ML Cohen SG Louie 1994 Chiral tubules of hexagonal BC_2N N Phys Rev B 50 4976 4979 https://doi.org/10.1103/PhysRevB.50.4976
8. X Blase J-C Charlier A Vita De R Car 1999 Structural and electronic properties of composite B x C y N z nanotubes and heterojunctions Appl Phys A Mater Sci Process 68 293 300 https://doi.org/10.1007/s003390050891

9. XD Bai J Yu S Liu EG Wang 2000 Role of nickel particles in selected growth of boron carbonitride tubular structures Chem Phys Lett 325 485 489 https://doi.org/10.1016/S0009-2614(00)00705-3
10. MA Mannan T Kida H Noguchi 2009 Atomic arrangement, composition and orientation of hexagonal BCN films synthesized by radiofrequency plasma enhanced CVD J Ceram Soc Jpn 117 503 507 https://doi.org/10.2109/jcersj2.117.503
11. CY Zhi XD Bai EG Wang 2004 Boron carbonitride nanotubes J Nanosci Nanotechnol 4 35 51 https://doi.org/10.1166/jnn.2004.018
12. CY Zhi XD Bai EG Wang 2002 Raman characterization of boron carbonitride nanotubes Appl Phys Lett 80 3590 3592 https://doi.org/10.1063/1.1479207
13. R Arenal X Blase A Loiseau 2010 Boron-nitride and boron-carbonitride nanotubes: synthesis, characterization and theory Adv Phys 59 101 179 https://doi.org/10.1080/00018730903562033
14. D Chen Y Huang X Hu R Li YL Qian 2018 Green synthesis of boron carbonitride with high capacitance Materials 11 387 https://doi.org/10.3390/ma11030387
15. CY Zhi JD Guo XD Bai EG Wang 2002 Adjustable boron carbonitride nanotubes J Appl Phys 91 5325 5333 https://doi.org/10.1063/1.1459596
16. W An CH Turner 2010 Linking carbon and boron-nitride nanotubes: heterojunction energetics and band gap tuning J Phys Chem Lett 1 2269 2273 https://doi.org/10.1021/jz100753x
17. M Machado T Kar P Piquini 2011 The influence of the stacking orientation of C and BN stripes in the structure, energetics, and electronic properties of BC 2 N nanotubes Nanotechnology 22 205706 https://doi.org/10.1088/0957-4484/22/20/205706
18. H Pan YP Feng J Lin 2006 Ab initio study of single-wall BC 2 N nanotubes Phys Rev B 74 045409 https://doi.org/10.1103/PhysRevB.74.045409
19. J Garel C Zhao R Popovitz-Biro 2014 BCN nanotubes as highly sensitive torsional electromechanical transducers Nano Lett 14 6132 6137 https://doi.org/10.1021/nl502161h
20. E Zahedi 2011 Size-dependent electronic structures of boron carbonitride (BC2N) nanotubes A DFT approach Superlattices Microstruct 50 491 500 https://doi.org/10.1016/j.spmi.2011.08.011
21. AR Juárez EC Anota HH Cocoletzi 2017 Stability and electronic properties of armchair boron nitride/carbon nanotubes Fullerenes Nanotub Carbon Nanostruct 25 716 725 https://doi.org/10.1080/1536383X.2017.1389905
22. A Soltani Z Azmoodeh MB Javan 2016 A DFT study of adsorption of glycine onto the surface of BC2N nanotube Appl Surf Sci 384 230 236 https://doi.org/10.1016/j.apsusc.2016.04.162
23. AS Ghasemi MR Taghartapeh A Soltani PJ Mahon 2019 Adsorption behavior of metformin drug on boron nitride fullerenes: thermodynamics and DFT studies J Mol Liq 275 955 967 https://doi.org/10.1016/j.molliq.2018.11.124
24. P Nematollahi EC Neyts 2018 A comparative DFT study on CO oxidation reaction over Si-doped BC2N nanosheet and nanotube Appl Surf Sci 439 934 945 https://doi.org/10.1016/j.apsusc.2017.12.254
25. M Akhavan S Jalili J Schofield 2015 Effect of diameter and chirality on the structure and electronic properties of BC2N nanotubes Chem Phys 455 88 93 https://doi.org/10.1016/j.chemphys.2015.04.018
26. C-K Yang 2011 Exploring the interaction between the boron nitride nanotube and biological molecules Comput Phys Commun 182 39 42 https://doi.org/10.1016/j.cpc.2010.07.040
27. BR Goldsmith JG Coroneus VR Khalap 2007 Conductance-controlled point functionalizartion of single-walled carbon nanotubes Science 315 77 81 https://doi.org/10.1126/science.1135303
28. Z Peralta-Inga P Lane JS Murray 2003 Characterization of surface electrostatic potentials of some (5,5) and (n,1) carbon and boron/nitrogen model nanotubes Nano Lett 3 21 28 https://doi.org/10.1021/nl020222q
29. P Politzer P Lane JS Murray MC Concha 2005 Comparative analysis of surface electrostatic potentials of carbon, boron/nitrogen and carbon/boron/nitrogen model nanotubes J Mol Model 11 1 7 https://doi.org/10.1007/s00894-004-0202-0
30. M Noei AA Peyghan 2013 A DFT study on the sensing behavior of a BC2N nanotube toward formaldehyde J Mol Model 19 3843 3850 https://doi.org/10.1007/s00894-013-1922-9
31. CJ Rupp J Rossato RJ Baierle 2009 First principles study of Si-doped BC2N nanotubes J Chem Phys 130 114710 https://doi.org/10.1063/1.3089357
32. Frisch M , Trucks G, Schlegel H, Scuseria G, Robb M, Cheeseman J, Scalmani G, Barone V, Mennucci B (2009) Gaussian 09, Revision A.1
33. Y Zhao DG Truhlar 2008 The M06 suite of density functionals for main group thermochemistry, thermochemical kinetics, noncovalent interactions, excited states, and transition elements: two new functionals and systematic testing of four M06-class functionals and 12 other function Theor Chem Acc 120 215 241 https://doi.org/10.1007/s00214-007-0310-x
34. AD McLean GS Chandler 1980 Contracted Gaussian basis sets for molecular calculations: I—second row atoms, Z=11-18 J Chem Phys 72 5639 5648 https://doi.org/10.1063/1.438980
35. AH Pakiari 2017 Geometric and electronic structures of vanadium sub-nano clusters, Vn (n = 2–5), and their adsorption complexes with CO and O2 Ligands: a DFT-NBO study Phys Chem Res 5 601 615 https://doi.org/10.22036/pcr.2017.80624.1364
36. J Jellinek 1999 Theory of atomic and molecular clusters Springer Berlin
37. RG Parr 1989 Density-functional theory of atoms and molecules Oxford University Press New York
38. RS Mulliken 1934 A new electroaffinity scale; together with data on valence states and on valence ionization potentials and electron affinities J Chem Phys 2 782 793 https://doi.org/10.1063/1.1749394
39. JP Foster F Weinhold 1980 Natural hybrid orbitals J Am Chem Soc 102 7211 7218 https://doi.org/10.1021/ja00544a007
40. AE Reed RB Weinstock F Weinhold 1985 Natural population analysis J Chem Phys 83 735 746 https://doi.org/10.1063/1.449486
41. T Kar M Čuma S Scheiner 1998 Structure, stability, and bonding of BC2N: an ab initio study J Phys Chem A 102 10134 10141 https://doi.org/10.1021/jp982424+
42. Z Zhou J Zhao X Gao 2005 Do composite single-walled nanotubes have enhanced capability for lithium storage? Chem Mater 17 992 1000 https://doi.org/10.1021/cm048746+
43. MO Watanabe S Itoh K Mizushima T Sasaki 1996 Bonding characterization of BC 2 N thin films Appl Phys Lett 68 2962 2964 https://doi.org/10.1063/1.116369
44. D Golberg P Dorozhkin Y Bando 2002 Semiconducting B-C–N nanotubes with few layers Chem Phys Lett 359 220 228 https://doi.org/10.1016/S0009-2614(02)00536-5
45. S Mukhopadhyay RH Scheicher R Pandey SP Karna 2011 Sensitivity of boron nitride nanotubes toward biomolecules of different polarities J Phys Chem Lett 2 2442 2447 https://doi.org/10.1021/jz2010557